EFDA–JET–PR(11)09

A. Simonetto, C. Sozzi, S. Garavaglia, J.A. Fessey, S. Nowak
and JETEFDA contributors

A Fast Multi-Channel Martin-Puplett Interferometer for Electron Cyclotron Emission Measurements on JET

A Fast Multi-Channel Martin-Puplett Interferometer for Electron Cyclotron Emission Measurements on JET

A. Simonetto[1], C. Sozzi[1], S. Garavaglia[1], J.A. Fessey[2], S. Nowak[1]
and JET EFDA contributors*

JET-EFDA, Culham Science Centre, OX14 3DB, Abingdon, UK

[1]Istituto di Fisica del Plasma CNR, Euratom-ENEA-CNR Association, 20125 Milano Italy
[2]EURATOM-CCFE Fusion Association, Culham Science Centre, OX14 3DB, Abingdon, OXON, UK
** See annex of F. Romanelli et al, "Overview of JET Results",*
(23rd IAEA Fusion Energy Conference, Daejon, Republic of Korea (2010)).

Preprint of Paper to be submitted for publication in
Review of Scientific Instruments

ABSTRACT

A Martin Puplett Interferometer for Electron Cyclotron Emission (ECE) measurements from JET tokamak plasmas was extended to multichannel operation for simultaneous radial and oblique ECE measurements. The paper describes the new optics and the instrument performance.

1. INTRODUCTION

Electron Cyclotron Emission (ECE) has been a standard diagnostic for electron temperature in tokamak plasmas for many years [1,2,3]. Most ECE systems developed recently have their strong point in the high time and spectral resolution achievable with heterodyne radiometers. However such systems require an impractically large number of channels with corresponding cost and complexity when accessing physical information requires a spectral coverage spanning two or more harmonics of the fundamental emission.

This is the case of studies aiming at the investigation of possible non-thermal features of the electron distribution function in high temperature tokamak plasmas, suggested by several experiments. The observation along multiple, oblique lines of sight of the second and third harmonic has been recognized in recent years as potentially useful in such investigations [4].

A single-channel fast-scanning Martin Puplett Interferometer (MPI) for ECE measurements of tokamak plasmas already in use at JET [5] was fitted with new optics, transforming it into a multichannel instrument for fast nearly synchronous measurements of radial and oblique ECE [6].

2. SYSTEM LAYOUT

Plasma emission is collected with three different antennas connected to transmission lines of about *60m*.

Oblique ECE is collected along two lines of sight *(≈10* and *≈25* degrees off the poloidal plane) through quasi-optical antennas [7] in Octant 8, and transmitted to the instrument through oversized circular copper waveguide with a diameter of *27.75mm*, with *17* mitre bends.

A square open-ended waveguide at major radius *4.1m* collects radial ECE for temperature measurements in JET's Octant 7. The transmission line is made with WR284 *(72.136×34.036 mm)* rectangular waveguide used as a "tall waveguide" in TE_{01} mode [8], with seven E-plane and seven H-plane mitre bends.

The transmission lines are fitted with manual switches near the MPI, that allow feeding the instrument either with the plasma emission or with radiation from a blackbody calibrator through a short (about *5m)* dedicated transmission line. This arrangement allows periodic relative calibration checks.

A cryostat holding six InSb detectors at liquid helium temperature is close to the instrument. Each detector is connected to the optics with a transmission line, made of *12mm* diameter copper pipe (about *1.5m)* with three mitre bends.

3. OPTICAL SCHEME

The frequency range of interest is *75* to *400GHz*, the upper frequency corresponding to third harmonic emission at half minor radius on the high field side or fourth harmonic on axis.

Since radiation emitted from the plasma in off-radial directions is elliptically polarized, two independent linearly polarized beams should be measured for each oblique line of sight. As a result, a minimum of five channels was required for the instrument. The optics design allows implementing six.

All channels share the existing wheel-shaped four-sector spiral rooftop reflector, that spins in the vertical plane at about *2200rpm*, allowing a path scan of almost *40mm* four times per turn, with a spectral resolution of up to *7.4GHz*.

The input waveguides for the off-radial channels are horizontal, facing the spinning mirror, with principal polarization planes (corresponding to the polarizations perpendicular/parallel to vacuum toroidal field) at *45* degrees from vertical, as a result of a suitable choice in waveguide routing.

The optical scheme [9] is sketched in figure 1. It relies on confocal telescopes (items 3,4 and 13,14 in the figure) producing an image of frequency-independent size of the input waveguide on the rooftop reflectors and on the output waveguide. The goal was obtaining an optical system as broadband as possible. The optical surfaces were dimensioned using coherent Gaussian beam optics (see e.g. [10]), with *a posteriori* geometric optics verifications on the field of view. The beam waist was placed at the waveguide aperture (diameter *27.75mm)* and chosen as *10.66mm* i.e. *0.768* times its radius r, for optimum coupling with a TE_{11} circular-waveguide mode (see e.g. [11]). This choice is based on the assumption that ohmic loss should cause a prevalence of the linearly polarized mode with lowest attenuation at the end of the transmission line, and an almost unimodal field would have a nearly flat phase front if reflections at the aperture are neglected. The truncation parameter is thus $2r/w=2.6$, preserved throughout the optical system over nearly all the band of interest.

Given the similarity between the diameter of the input waveguide and the transverse dimension *(30 mm)* of the movable rooftop reflector, a unit magnification was chosen for the *input* confocal telescope, that images the input waveguide on the two rooftop reflectors. The *output* telescope has magnification *0.43* in order to image the beam waists at the rooftop reflectors on the aperture of the output waveguide, a *12 mm* diameter copper pipe leading to the detectors. The choice of the pipe diameter was constrained only by the size (*20 mm)* of the (individual) detector windows on the dewar and the maximum cutoff frequency. Calculations show that ohmic attenuation in the pipe, while detrimental to signal to noise ratio, is not critically dependent on a reasonable choice in diameter.

Off-axis ellipsoidal mirrors (four per channel, three identical) designed for 90 degree reflection were used for the focussing optics. The radius *(150 mm)* of the rotating rooftop reflector and the requirement to fit six channels along the circumference constrain the focal length of the input mirrors, and *200mm* were chosen as a reasonable compromise between compactness and feasibility. The last mirror (the second of the output telescope) must then have a focal length of about *86.5mm*.

The curvature radii R

$$R = z + \frac{1}{z}\left(\frac{kw_0^2}{2}\right)^2 \tag{1}$$

where z is the distance from the beam waist, k is the propagation constant and w_0 is the waist size, were computed near midband *(250GHz)* at the location of the centres of the mirrors, and used for the definition of the ellipsoids.

The corresponding beamwidth w is

$$w = w_0\sqrt{1+\left(\frac{2z}{kw_0^2}\right)^2} \tag{2}$$

where the symbols have the same meaning as in equation (1). The transverse size h of the mirrors is 50mm square, which satisfies the condition on beam truncation $h/w \geq 2.6$ over most of the bandwidth.

The transverse mirror size limits the resolving power $\nu/\Delta\nu \approx 8(f/h)^2$ (see e.g. [12]), where f and h are the mirrors' focal length and diameter, to about *128* as a consequence of field curvature.

The transmission line for radial view second harmonic X-mode ECE is a rectangular waveguide used in TE_{01} mode. A *400mm* H-plane linear up-taper transforms it into a square waveguide. The input confocal telescope is made with a parabolic mirror of *480mm* focal length, placed at *100mm* in front of the waveguide, and an ellipsoidal mirror of *200mm* focal length (items 6 and 4 in figure 1). This arrangement is a compromise to save space and keep the optics simple.

The rectangular waveguide would couple efficiently [13] (up to *88%* power transfer) with an elliptical beam (waists *0.35a* and *1.07b*, *a,b* being the long and short sides of the waveguide), that would require two cylindrical mirrors for broadband matching with a circular beam. The *72mm* square waveguide would require an ellipsoidal mirror of *583.3 mm* focal length for optimum power transfer *(84%)* to a beam of waist *0.43a*. The parabolic mirror close to the waveguide should have the same focal length, but the beam with optimum coupling hits the limit of maximum throw: the beam radius at the mirror is only *31.1mm*, giving a maximum throw $kw^2/4 = 505.6mm$, lower than the focal length required. A compromise was accepted, using a shorter but feasible focal length of *480mm*, and accepting reduced coupling *(80%* in power) to a beam with a larger waist *(25.58mm*, i.e. *0.355 a)*. This beam also experiences larger truncation at the moving reflector (truncation parameter 2.32) but the increase in coupling loss is negligible.

The parameters of the mirrors are reported in Table 1, where the name "input" is used for the fixed waist (set by waveguide size) and "output" is the frequency dependent one.

The circular waveguides feed two channels each, since oblique plasma emission is not linearly polarized. Channel splitting is achieved with a wire-grid polarizer between the two mirrors of the input telescope, branching a second beam at 90 degrees from the input one. But the dominant TE_{11} mode in circular waveguide is not linearly polarized away from the waveguide axis, and some inter-channel crosstalk due to higher-order Gaussian modes is thus unavoidable.

A metal plate covered with Eccosorb AN72 is placed near the polarizer grid for each channel, in order to feed a definite room-temperature emission into the secondary input port.

The orientation of the last mirror before the rooftops takes care of perpendicular incidence of the beams onto the spiral reflector. As a consequence, this mirror is used with a different (channel-dependent) angle of incidence from the 45 degrees it was designed for. The cost saving in making it identical to the others was deemed compelling with respect to the negligible resulting aberration. The angle between the two branches derived from a single input waveguide was chosen as 90 degree to simplify the layout. But in order to obtain a proper 90 degree rotation upon reflection on a rooftop, the input polarization must be of course at 45 degrees to the symmetry plane, which sets the orientation of the beamsplitter grids. Our choice of the angle between branches pertaining to the same waveguide prevents proper matching of the beam polarization with the orientation of the beamsplitter grids, leading to an error of *5.9* and *7.0* degrees for the two branches. This gives rise to an imbalance between the reference and movable arms of the interferometers, resulting in lower fringe amplitude. The power imbalance is 39.8/60.2% and 62.1/37.9% in the two branches, but the reduction in fringe amplitude is only *2* to *3%* with respect to the ideally balanced case, so no corrective action was taken and the slight reduction in performance was accepted in exchange for a simpler layout. Electromagnetic tests were made to check these numbers, and a good agreement was obtained [14].

The two pairs of oblique channels were located in radially symmetric positions with respect to the (horizontal) spin axis of the spiral mirror, placing the beam splitters in the horizontal plane. Enough room was left in front of the central portion of the spinning mirror for placing two radial channels on opposite sides of the vertical diameter.

Given the space made available by the large focal length of the parabolic mirror, a flexible configuration was used for the radial-view channels, inserting a suitable set of plane mirrors that allows to feed two beams with both polarizations of the input rectangular waveguide or to use an identical independent waveguide. Again, a small polarization error of *11.2* degrees is obtained, resulting in a power imbalance of *69.1/30.9%*, but a fringe amplitude reduction of less than *8%*, that again was deemed acceptable.

4. MECHANICAL LAYOUT

All the components of the input telescope for oblique channels and the last mirror for the radial ones lie on a vertical plane, perpendicular to the rotation axis of the spinning mirror. A single *0.9×1m* aluminum plate *15mm* thick supports them all, using small wedge-shaped adapters for supporting mirrors that are not parallel to it. Dowel pins grant the alignment. Electromagnetic simulations with GRASP [15] suggest that a positional accuracy of *0.1mm* and *0.05 degrees* is required. But practical considerations prevented the use of interference coupling in the dowel pins, so their tolerance was usually set to *0.1 mm,* that grant a reasonable ease of assembly/disassembly, placing them as far apart as possible on the coupling parts in order to increase the critical angular tolerance. In actual

facts, as shown in the final discussion, the instrument turned out more resilient to misalignments than the simulations. The last piece of input waveguide is included in the optics and mounted onto the same support plate to reduce alignment errors.

The beamsplitter wire-grids, the reference rooftop mirrors and the output telescopes share the other side of the support plane, the six channels differing only in mechanical layout, in order to fit everything in a small space. Upon reflection at the last elliptical mirror, the beams traverse the mounting plane again to cross the small analyzer grids and enter the circular waveguides that lead to the detectors' cryostat. A special modification was made on the output of the radial channels to allow the radiation reflected by the analyzer grid being collected with a waveguide. When using a single rectangular input waveguide in a single polarization, this allows using the sixth detector to give some redundancy with a potential increase in signal to noise ratio.

The optics required for the radial channel was fitted to a second vertical metal plate *(0.5 × 0.9m)*, connected to the other in a solid T-shaped arrangement (with struts). The rigid layout allows lifting and moving the whole optics without loss of internal alignment, which is especially important, given the large number of components. This arrangement is also very stable against degradation induced by motor vibration.

An optical table hosts the motor, spinning wheel and the optics, which is mounted on self-centering supports, the position reference with respect to the moving rooftop reflector being set with a spacer holding on the motor bearing support.

A vibration sensor [5] monitors the spinning wheel continuously, providing an interlock to the motor to prevent any mechanical problems to grow into damage. Normal values of vibration are of the order of *0.05G* and the alarm threshold is lower than 0.3G.

Since the moving rooftop is spinning at about *2200rpm*, any failure to its assembly bolts would pose a significant safety risk. Therefore a cylindrical aluminum enclosure with very thick side wall, tightly bolted on a stainless steel base, was placed around the spinning wheel to contain any debris in the unlikely event of a catastrophic mechanical failure accompanied with a fault at the control circuitry. With this cover the maximum speed authorized in safety is 4000 rpm, allowing a time resolution up to about 4 ms per interferogram. Higher speeds are prevented by elastic structural deformation of the moving reflector [16].

The front holes for beam access were covered with thin plastic windows for safety (tamper prevention), dust avoidance and acoustic noise reduction. Windows pose no significant reflection problems, since the incidence of the beams is *4.85deg* off normal. Their transmission, shown in figure 5, was computed from the ratio of the measured spectrum of a blackbody source with and without window.

To aid instrument maintenance, a permanent laser alignment facility was built into the last part of transmission line for local calibration, using optically polished mirrors in the last few mitre bends. More details on the mechanical layout are given in [14].

5. DATA ACQUISITION

The existing data acquisition system [5] was upgraded too, preserving the original configuration as a backup solution in case of encoder failure. The spinning mirror position is measured with a 12-bit encoder on the motor shaft. The encoder signal is frequency-divided by four to drive the speed-independent sampling of 1024 samples per turn, setting the Nyquist frequency at about $0.95\ THz$, well above the fourth harmonic emission range of JET plasmas. The encoder *Z*-pulse is used to trigger a LeCroy 4433 CAMAC latching scaler that counts JET's data acquisition system 1 MHz clock and the sampling pulses. The latter signal provides information on the position of the wheel at the initial trigger, having of course a constant value of 1024 samples/turn afterwards (deviations from the constant value are then an early monitor of mechanical problems). The former signal allows timing information to be reconstructed, thus providing also an absolute measure of rotation speed. The independent optical sensor previously used [5] for driving the latching scaler is digitized together with the detectors' output on an INCAA PCI-TR22-5618 14-bit ADC, thus providing early evidence for encoder slippage.

6. TESTS AND CALIBRATION

The optical system throughput, defined as the fraction of input power delivered to the output waveguide (leading to the detector), was measured with a modulated solid-state WR6 noise source, and the result confirms simulations made using coherent radiation in the physical optics approximation with GRASP.

An absolute calibration, whose details will be reported elsewhere, was made by placing a blackbody source built at JET [17] inside the vessel, in front of each antenna in turn. A shutter covered with TK Tessalating RAM [18] was raised under remote control between the antenna and the source, to act as the cold reference. The remote control system allowed switching between the two sources to apply the standard two temperature calibration method. But only a fraction of data were actually collected by switching reference over alternate datasets, the vast majority using a single manual commutation over the integration period. This increased the effect of changes in the environment temperature, but the impact of this systematic error is below the noise level, according to estimates based on ambient temperature records in the rooms traversed by the transmission line. Data were collected and stored directly on disk for off-line processing. Spin-synchronous average and standard deviation were computed over single data units of about 30 minutes. The stability of standard deviations as a function of the number of turns allows them to be treated as error bars on individual data points.

Data processing of individual interferograms is fairly standard, consisting in Fourier tranforming a short bidirectional portion, obtaining the precise location of the Zero Path Difference feature from the amplitude-weighted slope of phase versus frequency, and the corrective phase term compensating for small misalignments and non idealities (see e.g. [19,20,21]) from a piecewise parabolic spline on the non–linear residual of the same curve. A cosine window is applied to the data, and the bidirectional

portion of interferogram is weighed with a linear function to avoid considering this portion twice in the Discrete Fourier Transform (DFT). The sine and cosine terms of the DFT are combined with the phase shifts computed above to obtain the even part of the one-sided interferogram. Error bars on spectra are computed with usual error propagation from the standard deviation of individual data sets, neglecting the covariance matrix of data. The process is described with all the details in [22] and references therein.

Averaged quantities of different data sets are combined using weights proportional to the number of turns. The resulting fractional error bar, with *80* hours integration time on hot and *20* on cold source, is shown in figure 6 in a representative case. Extrapolation to plasma measurements gives a signal to noise ratio about 50 times better than the one shown in the figure, which is in fair agreement with estimates obtained with different techniques [6,23]. Local calibrations have a S/N ratio about 20 dB better than in-vessel ones, because of the attenuation in the long transmission line. The measurements shown in figure 5 were obtained with an integration time of 20 minutes.

7. DISCUSSION

The performance obtained is summarized in table 2, where the relevant quantities are listed.

The instrument is less sensitive than the venerable single channel MPI [25] used at JET since its beginning more than 25 years ago. This is explained by the difference in the input transmission lines and the presence of the output waveguides, whose loss is about 6dB, which are directly subtracted from the signal to noise ratio. Avoiding them would have required either a horizontal-mount dewar or a complete redesign of the instrument, making the spiral rooftop mirror spin horizontally below the detectors.

Another design choice that needs justification is the use of mirrors instead of lenses. The design philosophy has been that of an essentially alignment-free optical system. The use of lenses would have made optical alignment checks a lot easier, but ad-hoc mounts compensating for the relatively large tolerance in lens diameter would have been required and aligned. The use of flat mirrors would have been anyway unavoidable to allow circular waveguides to feed two channels each, and to accommodate five (six) channels within the small diameter of the spinning mirror.

There is no evidence so far for a need of periodic realignment. When the spinning mirror had to be unmounted because of a failure (due to normal wear) of the ball bearing during in-vessel calibration, no realignment was performed, leaving the instrument in a status that was still perfectly compatible with operation, albeit detectably different, as evidenced by an apparent displacement in the water lines. The frequency displacement of the lines is due of course to the increase in optical path along the moving arm of the interferometer, induced by the small misalignment, with respect to the normal almost *40 mm*. It is different for the four sectors, showing that the rotation and symmetry axes of the wheel are not *perfectly* aligned. The path difference is changed up to *≈1.5%* as a result of the different trajectories of the shifted and reference beams in the optical system, but the data are perfectly usable, provided that one accounts (once for all) for the effective path variation in

generating the frequency axis of the spectra, e.g. using the position of the many absorption lines of water vapour in this frequency range [24], that are clearly visible in local calibration. Further details are available in [23].

More statistics with plasma data is required to assess the accuracy limits of the instrument with the recent absolute calibration, but it has offered so far a stable and reliable operation with significant improvements in temporal and spectral resolution with respect to the existing interferometer. The signal to noise ratio could be improved with moderate effort for the most critical channel (radial view, used for temperature measurements) using a 2-3 mirror quasi-optical transmission line instead of the output waveguide.

ACKNOWLEDGMENTS

We are indebted with P. Trimble for his precious technical assistance and to S. Schmuck for his essential contribution to the absolute calibration. This work was supported by EURATOM and carried out within the framework of the European Fusion Development Agreement Tasks JW4-NEP-ENEA-37, JW4-OEP-ENEA-42B, TW6-THE-MWA EFDA/06-1531. The views and opinions expressed herein do not necessarily reflect those of the European Commission.

REFERENCES

[1]. F. Engelmann and M. Curatolo, Nuclear Fusion **13**, 497 (1973)

[2]. A.E. Costley, R. J. Hastie, J. W. M. Paul and J. Chamberlain, Phys. Rev. Lett. **33**, 758 (1974)

[3]. A.E. Costley, Fusion Science and Technology, **55**, 1 (2009)

[4]. E. de la Luna, V. Krivenski, G. Giruzzi, C. Gowers, R. Prentice, J.M. Travere and M. Zerbini, Review of Scientific Instruments **74**, 1414 (2003)

[5]. M. Zerbini, P. Buratti, C. Centioli, J.A. Fessey, S. Nowak and JET-EFDA Contributors, *Interferometric Spectrometry in the Microwave range for High Resolution ECE Measurements,* 15th Conference on High Temperature Plasma Diagnostics, San Diego, (2004).

[6]. L. Figini, S. Garavaglia, E. De La Luna, D. Farina, P. Platania, A. Simonetto, C. Sozzi and JET-EFDA Contributors, Review of Scientific Instruments **81**, 10D937 (2010).

[7]. C. Sozzi, A. Bruschi, A. Simonetto, E. De La Luna, J.A. Fessey, V. Riccardo and JET-EFDA Contributors, Fusion Engineering and Design, **74**, 691 (2005)

[8]. E.A.M. Baker, D.V. Bartlett, D.J. Campbell, A.E. Costley, D.J. Daly, A. Dellis, L.C.J.M. De Kock, J. Fessey, *Overmoded millimeter waveguide transmission system for the JET ECE diagnostic*, Proceedings of EC-4 4th international workshop on ECE and ECRH, Roma, 1984, p. 11

[9]. A. Simonetto, C. Sozzi, S. Garavaglia, J.A. Fessey and JET EFDA contributors, *Conceptual Design Of The Optical Scheme For A Multichannel Martin Puplett Interferometer For Perpendicular And Oblique ECE Measurements On JET,* Proc. of the 14th Joint Workshop on ECE&ECRH, 238-242, A. Lazaros ed., Heliotopos Conferences Ltd. (2006)

[10]. P.F. Goldsmith, *Quasioptical Systems: Gaussian Beam Quasioptical Propogation and Applications,* IEEE Press Series on RF and Microwave Technology, 1997

[11]. J.A. Murphy, IEEE Transactions **AP-36**, 570 (1988)

[12]. R.J. Bell, *Introductory Fourier Transform spectroscopy,* Academic Press, 1972, New York, London

[13]. Beam coupling computed by maximizing the function $f(w_0) = \iint_A E_{WG} \cdot u_{00}(w_0) da$, where the integral is over the waveguide aperture A, E_{WG} is the field of the fundamental waveguide mode and $u_{00}(w)$ is the field of the first Gaussian mode. Since linearly polarized modes are considered, fields are represented as scalar quantities, and since the phase front is flat for a single waveguide mode and for a Gaussian beam with waist at the aperture, the integrand is real.

[14]. S. Garavaglia, A. Simonetto, C. Sozzi and JET-EFDA contributors, Fusion Engineering and Design, **82**, 1224 (2007).

[15]. http://www.ticra.com

[16]. Structural analysis by D. Starkey (CCFE)

[17]. Thermal design by V. Thompson (JET), mechanics by JET DO and control system by J. Fessey (CCFE)

[18]. Thomas Keating Ltd, http://www.terahertz.co.uk

[19]. L. Mertz, Infrared Physics **7,** 17 (1967)

[20]. H. Sakai, G.A. Vanasse and M.L. Forman, Journal Optical Society of America, **58**, 84 (1968)

[21]. C.D. Porter and D.B. Tanner, International Journal of Infrared and Millimeter Waves, **4**,273 (1983)

[22]. A.Simonetto, *MPISUB, a Fortran subroutine for processing Martin-Puplett interferometer data*, IFP internal report FP10/04(2010), available also online http://www.ifp.cnr.it/publications/2010/FP10_04.pdf

[23]. S. Garavaglia, J.A. Fessey, A. Simonetto, C. Sozzi and S. Schmuck and JET-EFDA contributors, *Performances of a Martin-Puplett interferometer for ECE measurements*, 26th Symposium of Fusion Technology, Oporto (PT), (2010).

[24]. R.H. Partridge, Journal of Molecular Spectroscopy **87**, 429 (1981)

[25]. A.E. Costley, E.A.M. Baker, D.V. Bartlett, D.J. Campbell, M.G. Kiff and G.F. Neill *First ECE measurements of ECE from JET*, Proceedings of EC-4 4th international workshop on ECE and ECRH, Roma, 1984, p. 1

Mirror focal length (mm)	"input" (constant) beam waist (mm)	"Input" curvature radius (mm)	"Output" curvature radius (mm)	output (variable) beam waist (mm) at (frequency (GHz))	beam radius at mirror (mm) at (frequency (GHz))
200	10.66	642.47	290.40	23.88 (75) 4.48 (400)	26.15 (75) 11.56 (400)
86.5	4.61	122.27	295.54	23.88 (75) 4.48 (400)	24.32 (75) 6.43 (400)
480 (parabolic)	25.58	-	480.00	23.88 (75) 4.48 (400)	26.05 (75) 25.59 (400)

Table 1: Mirror and beam parameters

Frequency range (GHz)	75 - 950
Path scan (mm)	40
Scans per revolution	4
Max/typ rotation speed (rpm)	3000/2200
Min/typ scan time (ms)	5/6.8
Max spectral resolution (GHz)	7.4
Interferograms per shot per channel	≈3000
Samples per interferogram	256
Max electrical bandwidth (kHz) Nyquist freq	25
Channels	6

Table 2: Summary of most significant performance parameters

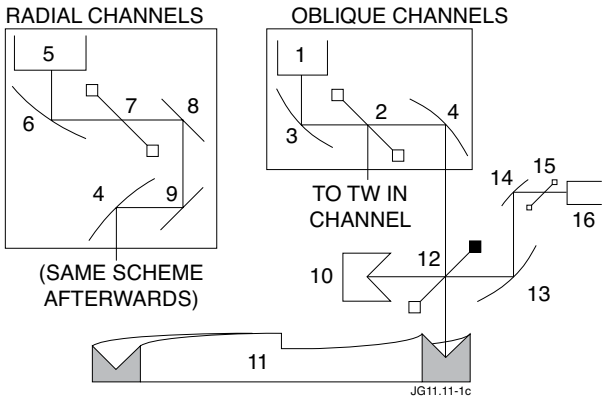

Figure 1: schematic drawing of the optics. Radiation from the circular input waveguide for oblique channels (1) is split with grid (2) in the two polarizations feeding different channels (only one shown). Input radiation is coupled into the interferometer with a confocal telescope of unit magnification, made with two identical elliptical mirrors (3,4). The square input waveguide for radial channels (5) is coupled to the interferometer with a parabolic mirror (6) and a set of plane ones (8,9). An elliptical mirror (4) identical to those of the oblique channels completes the input telescope in this case, radiating into the interferometer a beam identical to those of the oblique channels. A grid (7) can be inserted along the beam path to branch another channel if the waveguide is used in dual polarization. The interferometer is made with the beamsplitter grid (12), the reference (10) and moving (11) rooftops. The output beam is focussed with a confocal telescope (13,14) into the analyser grid (15) and the output waveguide (16) leading to the detector (not shown). Mirror (13) is identical to (3,4).

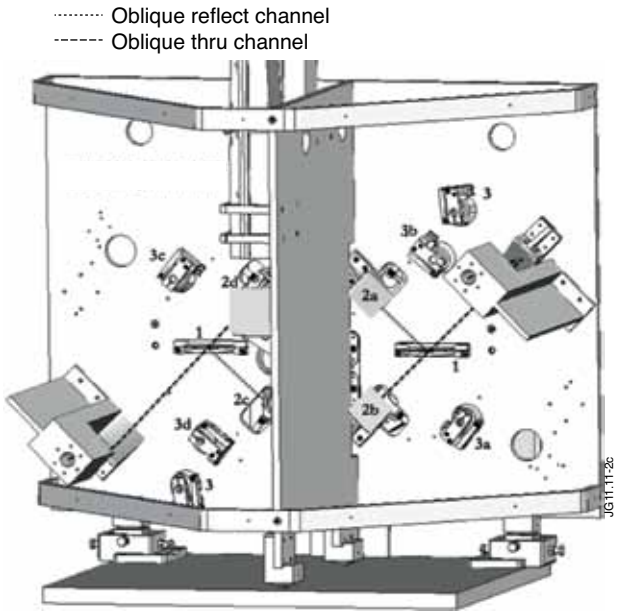

Figure 2: Principal support plane, front view. Radiation coming from the circular waveguides is split with the beamsplitter wire-grids (1) in two orthogonally polarized beams feeding different channels (thru, b & d and reflect, a & c). Input radiation is sent to the interferometer on the opposite side of the plane with an ellipsoidal mirror (2) (Mirror 2c removed to show access hole). The output beam crosses the analyzer grid and enters into the output waveguide (only support is shown) (3) leading to the detector (not shown).

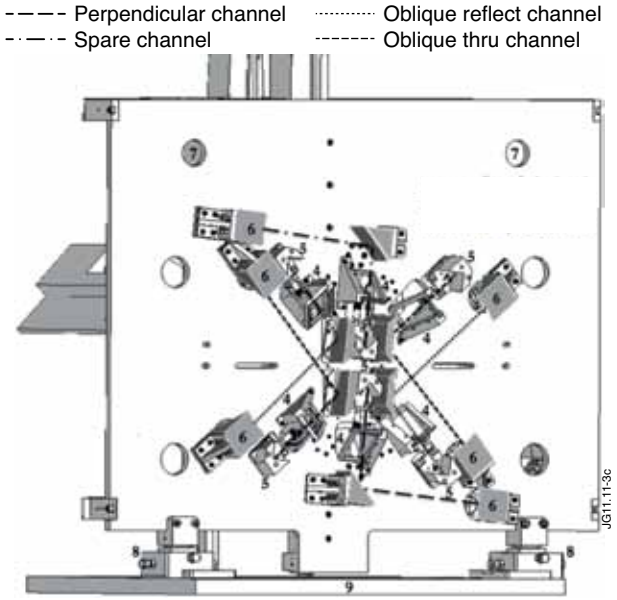

Figure 3: Principal support plane, rear side, facing the spinning mirror. Radiation coming from the front side is sent to the reference (5) and moving rooftops (the spinning wheel) through the beamsplitter grid (4). Cross-polarized reflected beams are recombined on the grid (4) and sent with elliptical mirrors (6) to the output waveguides, back on the other side of the plane. Lifting holes (7) are provided for a crane sling and (8) the slides to adjust the position on the optical table (9).

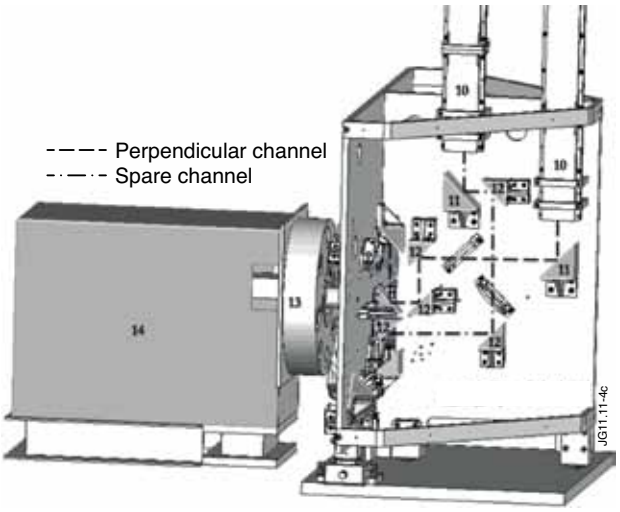

Figure 4: Mid-plate. Two rectangular input waveguides are dedicated to radial channels. Input radiation is sent to the interferometer through a taper (10) with a parabolic mirror (11) and a set of plane ones (12). Re-configuration of the plane mirrors (mounting holes already in place) allows to choose between measuring radiation from two independent waveguides or the two polarizations of the same waveguide. In this case the only connected waveguide carries a single polarization (a polarizer is present near the antenna) so the detector of the spare channel is used to improve the signal-to-noise ratio of the radial channel (see text above). On the left the wheel protection (13) and the motor cover (14).

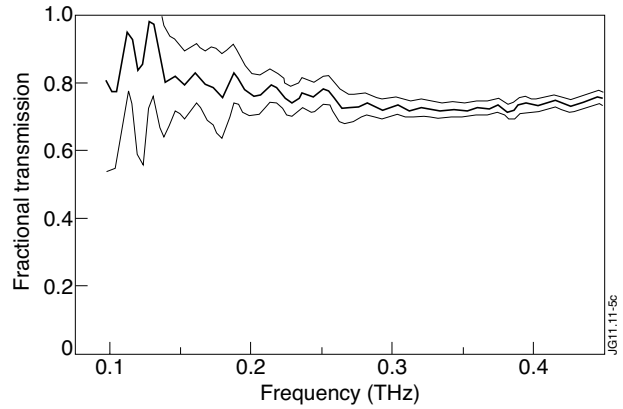

Figure 5: fractional power transmission of thin plastic windows over the frequency range of interest (thick trace), and 95% confidence interval (thin lines). Data quality is similar up to the Nyquist frequency (0.95THz) apart from regions including strong water vapour absorption lines (0.55-0.60, 0.75,0.79THz).

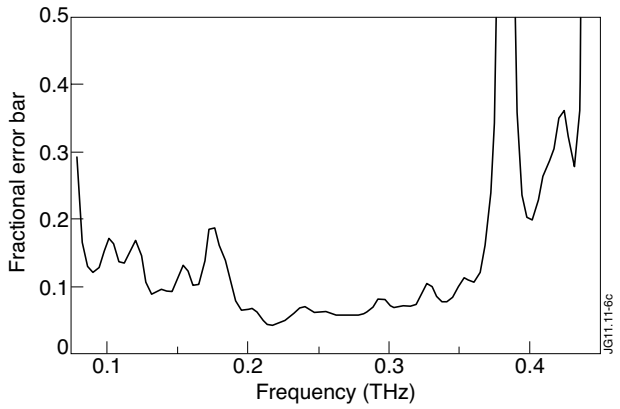

Figure 6: fractional error bar (67% confidence interval) in absolute in-vessel calibration of radial channel. Second harmonic ECE from plasma is normally limited to the range 100-300GHz. The large error bars at 0.38 and 0.45THz are due to water vapour absorption lines. See e.g. [24]. The fractional error bar exceeds 0.5 everywhere above 0.45THz, presumably because the transmission line attenuation is too large. Local calibrations show detectable signal up to the Nyquist frequency of 0.95THz.